J Membrane Biol (2010) 235:163–175
DOI 10.1007/s00232-010-9261-6

Statistical Analysis of High-Resolution Light Microscope Images Reveals Effects of Cytoskeleton-Disrupting Drugs on the Membrane Organization of the Nicotinic Acetylcholine Receptor

Jorge J. Wenz · Virginia Borroni · Francisco J. Barrantes

Received: 19 February 2010 / Accepted: 8 May 2010 / Published online: 8 June 2010

Abstract Extensive evidence supports the notion that the cytoskeleton participates in the immobilization and membrane clustering of the nicotinic acetylcholine receptor (AChR) at the neuromuscular junction. Stimulated emission depletion fluorescence microscopy has revealed the supramolecular organization of AChR nanoclusters at the surface of CHO-K1/A5 cells with subdiffraction resolution (Kellner et al., Neuroscience 144:135–143 2007). We studied the effect of two cytoskeletal-disrupting drugs (cytochalasin D and jasplakinolide) on the nanoscale distribution of muscle-type AChR expressed in these cells by means of mathematical and statistical analysis of images obtained with the same high-resolution microscopy. AChR nanoclusters were found to be randomly distributed in both controls and cells treated with either drug for distances larger than 500 nm. Treatments altered the distribution of AChR nanoclusters according to their brightness/size. Cytochalasin D and jasplakinolide produced a statistically significant increase in the proportion of medium-size nanoclusters and a diminution of small nanoclusters, indicating higher disrupting activity on the latter. This was further corroborated by the diminution of the brightness/diameter ratio of nanoclusters (a measure of the intracluster density of AChR molecules) and by Ripley's analysis applied to simulated patterns with intracluster aggregation of AChR molecules. The combined analytical tools bring out subtle changes in the two-dimensional organization of the AChR nanoaggregates on disruption of the cytoskeletal network and throw light on the possible link between the cytoskeleton and the distribution of the AChR at the cell surface.

Keywords Clustering · Statistical analysis · Ripley's test · Poisson · AChR · STED · Cytoskeleton

Increasing evidence supports the view that many membrane proteins are clustered at the cell surface, and that such clustering plays an important role in their functionality (Choquet and Triller 2003; Sieber et al. 2007). At the neuromuscular junction, fast and accurate synaptic transmission requires clustering of nicotinic acetylcholine receptors (AChRs), at concentrations ~1000-fold higher (i.e., 15,000–20,000 μm^2) than that at the contiguous extrasynaptic membrane (Barrantes 1983). The maintenance of this high density of receptors results from a balance between various mechanisms: increased local synthesis of new receptors, redistribution of existing surface receptors, decreased turnover and limitation of diffusion of aggregated receptors (Kummer et al. 2006), and trapping within corrals and fences provided by the extracellular matrix and the subcortical cytoskeleton.

Receptor clustering also involves interactions between postsynaptic proteins, among which agrin plays a key role (Kummer et al. 2006, and references therein). Agrin has been associated with elevated expression and targeting of rapsyn to the postsynaptic membrane, thereby packing more AChRs into stable, functionally AChR aggregates (Brockhausen et al. 2008). Reciprocally, the presence of AChR was reported to be required for agrin to induce clusters of other postsynaptic components, such as α- and β-dystroglycan, syntrophin isoforms, and rapsyn (Marangi et al. 2001).

Electronic supplementary material The online version of this article (doi:10.1007/s00232-010-9261-6) contains supplementary material, which is available to authorized users.

J. J. Wenz (✉) · V. Borroni · F. J. Barrantes
Instituto de Investigaciones Bioquímicas de Bahía Blanca and UNESCO Chair of Biophysics and Molecular Neurobiology, C.C. 857, F8000FWB Bahía Blanca, Argentina
e-mail: jwenz@criba.edu.ar

Another important factor in stabilizing AChR clusters at the neuromuscular junction is the cortical cytoskeletal network. Association of the AChR with the cytoskeleton involves phosphorylation of the β-subunit concurrently with the presence of agrin and rapsyn (Fuhrer et al. 1999; Marangi et al. 2001; Marchand et al. 2002; Sadasivam et al. 2005; Willman et al. 2006; Borges et al. 2008). AChR–cytoskeletal interactions are also operative in central nervous synapses: the neuronal α7 AChR colocalizes with the cytoskeletal protein F actin, and dispersion of F actin patches and α7-AChR clusters into smaller aggregates was observed after the cytoskeleton was selectively depolymerized (Brusés et al. 2001).

We have recently studied the cell surface organization of AChR in the mammalian CHO-K1/A5 cell line, which stably expresses adult muscle-type receptors. We have found that in this cell line AChR is organized as subdiffraction aggregates with sizes in the order of nanometers (Kellner et al. 2007). The organization of these aggregates is cholesterol sensitive; cholesterol depletion reduces the number of aggregates by accelerating their internalization and increases the size of the remaining ones (Borroni et al. 2007; Kellner et al. 2007) by a mechanism possibly involving the cytoskeleton (Kumari et al. 2008). In this work, we investigated the connection between the spatial distribution of the AChR and the cytoskeleton in CHO-K1/A5 cells. The effect of the cytoskeleton-disrupting drugs cytochalasin D (Cooper 1987) and jasplakinolide (Bubb et al. 1994) on the clustering behavior of the AChR macromolecule was assessed by stimulated emission depletion (STED) microscopy, a nanoscopy technique (see Hell and Wichmann 1994; Klar and Hell 1999) enabling imaging of AChR aggregates with subdiffraction resolution (reviewed in Barrantes 2007). In the present work, the light microscopy images were subjected to statistical and mathematical analyses, bringing out subtle changes in the 2-D organization of the nanoaggregates on disruption of the cytoskeletal network that are not revealed by simple observation of images.

Materials and Methods

Cell Culture

CHO-K1/A5 cells were grown in Ham's F12 medium supplemented with 10% fetal bovine serum for 2–3 days at 37°C before experiments as in Roccamo et al. (1999).

Labeling of CHO-K1/A5 Cells for Confocal and STED Microscopy

CHO-K1/A5 cells were labeled for 1 h with mAb210, a monoclonal antibody against the AChR α subunit, followed by staining for 1 h with a secondary antibody coupled to the fluorophore Atto^{647N}. Cells were then washed, fixed with 2% paraformaldehyde for 30 min at room temperature, and imaged in confocal and STED modes using a Leica TCS STED microscope at the microscopy facility of the Department of Nanobiophotonics (Prof. S. W. Hell, Max-Planck-Institute for Biophysical Chemistry, Göttingen) using excitation at 635 nm provided by a broadband Spectra-Physics MaiTai laser line. The nominal XY resolution (full-width half-maximum) in the STED mode was ~70 nm as compared to the approximately 250-nm lateral resolution in the confocal mode, whereas the resolution along the z-axis in the confocal and STED modes was ~550 nm full-width half-maximum.

Treatment of CHO-K1/A5 Cells with the Cytoskeleton-Disrupting Drugs Cytochalasin D and Jasplakinolide

CHO-K1/A5 cells were incubated for 30 min at 37°C with complete medium only (control), cytochalasin D (2.5 µmol/L), or jasplakinolide (1 µmol/L). At the end of the incubation period cells were labeled with monoclonal antibody mab210 as described above. Cells were subsequently imaged using the confocal and STED microscopy modes, respectively.

Processing of STED Images

The background fluorescence for each image was calculated as the average intensity +3 SD in cell-free regions and subtracted from each image. Before further analysis of AChR spots, addition of 3 SD to the average background ensured that no artefactual spots were taken into account. Regions of 5 × 5 µm were selected from each image excluding edges of cell membranes and cell-free zones (substrate cover glass). Depending on the size of the cells, regions were selected from the same or different cells in the same image. The number of processed images and AChR spots is listed in Supplementary Table 1. AChR spots were manually selected in each selected region using a custom-written MatLab routine, as in Kellner et al. (2007). Those spots having a brightness distribution that could not be adequately fitted by the Lorentz distribution ($\chi^2 > 0.03$) were not included in the analysis. The coordinate (x,y) of the spot was determined by the central point of the region of interest (ROI) using the same custom-written software.

Analysis of STED Images

Use of Three-Dimensional Euclidean Distances for Determining the Spatial Organization of AChR Nanoclusters According to Brightness

To investigate whether the spatial organization of AChR nanoclusters in the cell membrane depends on the

brightness of spots, and assuming that brightness is proportional to the number of particles in a spot, Euclidean distances (D) between each pair of spots were represented in a 3-D matrix (x,y, brightness). Supplementary Fig. 1 shows a selected 5 × 5-μm region on the plane of the membrane (x,y) with the average number of spots (25) per region, and their corresponding measured fluorescence intensity (brightness) in arbitrary units (AU). In order to equilibrate the weight of the variables x,y and brightness when computing the 3-D Euclidean distances, the values of these variables were normalized and placed in a box of 100 × 100 × 250 AU. The raw 2-D coordinates, or each spot in the plane of the membrane (x,y), originally in the interval of 0–5 μm, were normalized by the highest value for each series of experiments, and next confined to the interval 0–100 AU [(raw value/highest value) × 100]. Because brightness exhibits different absolute values (see Supplementary Table 2) and units relative to x and y, it was normalized by the mean [norm = (raw value/mean) × 50)] for each series of experiments (i.e., control, and cytochalasin D– or jasplakinolide-treated cells).

Because of the asymmetric distribution of the frequencies of this variable, with a long tail to the right side of the plot (see, e.g., Fig. 4 below), a small number of spots (<1%) with brightness higher than 250 AU was discarded from the analysis. From the transformed variables the 3-D Euclidean distances (amounting to ~64,000) were next computed by applying trigonometric criteria (Supplementary Fig. 1) between all pairs of spots within each set of samples (control, cytochalasin D, and jasplakinolide). The obtained frequencies were summed and binned in a general plot. It is worth noting that if normalization of brightness had been accomplished by dividing each element by the maximum value, confining all the elements in the 0–100 interval, most of them would be crowded at the lower limit of the interval, thus reducing the weight of the variable brightness in comparison to the other two variables (x,y), and hence lowering the sensitivity of this method. The same would occur if normalization of brightness were performed at higher values (i.e., norm (raw value/mean) × 100). The large number of spots with brightness higher than 100 would reduce sensibility of the method by overweighting this variable. Because they are computed from variables having different units and then normalized, Euclidean distances are unitless.

To interpret changes in the frequency plots resulting from the treatment of cells with cytoskeleton-disrupting drugs, the frequency distribution of Euclidean distances was next analyzed in simulated patterns having the same box size (5 × 5 μm) and average number of spots (25) as the actual STED micrographs of AChR particles (Fig. 1).

One hundred patterns of 25 points each were first generated with a random distribution of each variable (x,y, brightness). Variables x and y ranged from 0–100 AU, whereas brightness was set to vary between 0 and 250 AU. Accordingly, points were randomly distributed in a 100 × 100 × 250 AU box. An example of a simulated pattern of spots in a bidimensional x,y surface is illustrated

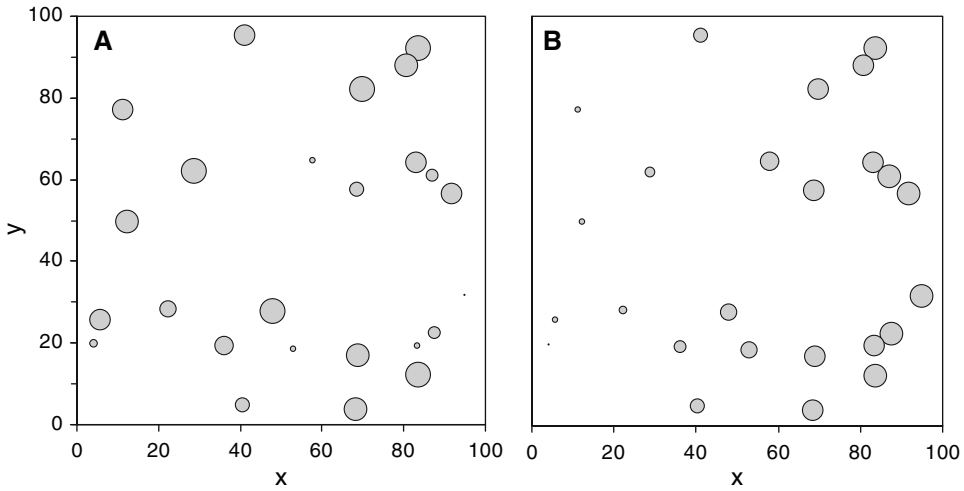

Fig. 1 Schematic depiction of simulated patterns of random and nonrandom distribution of 3-D Euclidean distances. **a** Scheme of an idealized image with the average number of nanoclusters (25) and random coordinates (x,y, brightness). The third coordinate (brightness) is represented by the area of the gray circle. Values of x,y vary from 0 to 100 and brightness between 0 and 250 (arbitrary units). **b** Keeping the same spatial distribution of nanoclusters in the x,y plane, brightness was redistributed by placing the lower values on the left side and the higher ones on the right side of the image. This redistribution of the brightness over identical x,y coordinates was used to estimate clustering of spots according to the brightness, independently of the 2-D distribution in the plane of the membrane (see Fig. 3). After generating hundreds of such patterns, Euclidean distances were calculated and binned in general frequency plots (see also Fig. 3)

in Fig. 1a, where the coordinates of each spot correspond to the center of each circle and the third variable (brightness) is represented by the area of the circles. Second, the hundred patterns of 25 points each were arranged according to their brightness, thus segregating larger spots (e.g., higher intensities to the right in Fig. 1b) from the smaller ones while keeping their x,y coordinates constant (Fig. 1b). Next the Euclidean distances were calculated for all pairs of points within all patterns. A total of 60,000 distances were computed for the 100 random and nonrandom patterns, a number similar to that observed in the experimental data (Supplementary Table 3), and were then summed and binned in an overall frequency plot.

Frequency Distribution of Brightness, Diameter, and Brightness/Diameter Ratio of AChR Nanoclusters

With respect to 3-D Euclidean distances, the mean normalized brightness (norm = (raw value/mean) × 50) was used next for constructing frequency histograms of brightness, instead of the raw values. The brightness of nanoclusters within each set of samples (control and treated) was binned into a general histogram that could be fitted by a log-normal type distribution. Analogously, diameters (averaged from the full-width half-maximum in the x and y coordinates) of nanoclusters within each set of samples were also binned and plotted. The brightness/diameter ratio was used as a measure of the intrananocluster density of particles. The ratio was computed for each spot, summed within each set of samples and plotted in an overall frequency histogram that could be fitted with a log-normal distribution.

The median was used as a measure of central tendency for these asymmetric frequency distributions because it is less sensitive to extreme values than the mean. For comparison of the frequency distribution between control and treated samples, the Wilcoxon test was performed (Statistica, version 6.0). This median- and dispersion-based method can be applied without the requirement of normal (needed for the *t*-test) and/or symmetrical frequency distributions.

Distribution of AChR Nanoclusters in the Plane of the Membrane

Ripley's Test

The spatial distribution of AChR clusters in the x,y plane was investigated by applying Ripley's analysis (Ripley 1977, 1979; Appleyard et al. 1985), which measures the number of particles within a given radius r of any given particle (Eq. 1):

$$L(r) - r = \sqrt{\frac{N(r)}{\pi D}} - r \tag{1}$$

where $N(r)$ is the number of particles within a distance r of a given particle, and D is the average particle density per unit area. Positive values of the function indicate clustering of particles, whereas values close to zero (± 1) are expected for a random distribution. Ripley's function was calculated using the Spatial Point Pattern Analysis (SPAA) software, version 2.0.3, and restricted to lengths (r) up to half the size of the selected regions (i.e., 2.5 μm). The central point of the ROI was used as the coordinate of the spot and $L(r) - r$ was calculated separately on each selected 5 × 5-μm region, followed by normalization by the 99% confidence interval (99% CI) for each r. Finally, the values of the function were averaged within each treatment. The 99% CI corresponds to the maximum value of Ripley's function obtained from 99 randomly simulated patterns having the same size and number of particles (i.e., equal density).

Poisson Distribution Analysis

The bidimensional distribution of AChR clusters in the plane of the membrane was also subjected to Poisson analysis. The field of the selected regions (5 × 5 μm) within images was divided uniformly into square boxes of 500 × 500, 1000 × 1000, and 2500 × 2500 nm, and clusters in each box were counted by subroutine written in Excel. Boxes with the same size and a given number of clusters (0, 1, 2, etc.) were counted and binned next into an overall frequency plot within each set of samples. The observed frequency distribution was compared with the Poisson (random) distribution (Eq. 2):

$$P(k, \lambda) = \frac{e^{-\lambda}\lambda^k}{k!} \tag{2}$$

where k is the number of clusters per box and λ is the mean number of nanocluster per box. The goodness of fit of the Poisson distribution to the observed frequencies was tested by the χ^2 statistic (Eq. 3):

$$\chi^2 = \sum_{i=0}^{n} \frac{\left(F_{\text{obs}} - F_{\text{exp}}\right)^2}{F_{\text{exp}}} \tag{3}$$

where F_{obs} and F_{exp} correspond to the observed and the expected frequencies (Poisson), respectively, and n corresponds to the number of bins with a frequency higher than 5 (a bin is a box with a given number of clusters—0, 1, 2, etc.). The χ^2 statistics were calculated for each individual bin and those bins having a frequency of >5 were next summed to obtain a general χ^2 for the entire frequency distribution. Differences between the observed frequency distribution and that for a random distribution were

meaningful at the corresponding level of significance (P) whenever the general χ^2 statistics was higher than a critical value (Chi_{crit}; see Fig. 6). A large value of χ^2 indicates a vanishing probability (P) that the observed distribution of spots in the membrane is consistent with a random distribution. The degrees of freedom used to compare between distributions were computed as $(n - 1)$.

Results

Organization of AChR Nanoclusters in CHO-K1/A5 Cells Revealed by STED Images

Confocal and STED microscopy images of CHO-K1/A5 cells double-labeled with monoclonal antibody mab210 against the AChR α subunit followed by a secondary antibody coupled to Atto^{647N} are shown in Fig. 2. Binding of antibodies promotes the cross-linking of AChR macromolecules and this results in the spotty appearance of the particles close to the resolution limit of the confocal microscope.

As stated in the Introduction, the cytoskeleton is an important regulator of protein organization at the cell membrane. In order to study the effect of the cytoskeleton on AChR cell-surface organization, CHO-K1/A5 cells were treated with drugs (cytochalasin D and jasplakinolide) that disrupt the organization of actin filaments (Supplementary Fig. 2). CHO-K1/A5 cells were incubated for 30 min at 37°C with cytochalasin D (2.5 µmol/l) or jasplakinolide (1 µmol/l), labeled as above and imaged. This relatively short incubation time allows these drugs to produce their effect on the cytoskeleton without altering the AChR cell-surface levels (Supplementary Figs. 2 and 3). Longer incubation periods (e.g., 2 h) with cytochalasin D inhibit AChR endocytosis in the CHO-K1/A5 cell line (Kumari et al. 2008). Furthermore, we have found that endocytic internalization of the AChR does not occur within this period (Kumari et al. 2008).

Spatial Organization of AChR Nanoclusters According to Their Brightness/Size

The frequency distribution of the 3-D Euclidean distances for the experimental data and for the simulated random and nonrandom patterns is shown in Fig. 3. We introduce this mathematical procedure to examine the spatial organization of the AChR nanoclusters according to their brightness/size. Treatment of CHO-K1/A5 cells with cytochalasin D or jasplakinolide (Fig. 3a) produced statistically significant changes in the relative frequency of Euclidean distances. Higher frequencies of distances around 30–70 AU were observed, and lower frequencies of distances larger than ~100 AU. It is worth noticing that the total area below the curves amounts to 100, and high values at certain distances must be counterbalanced by equivalent low values at other distances.

To interpret the experimentally observed changes, frequency distributions corresponding to the simulated random and nonrandom patterns were compared (Fig. 3b). The curve corresponding to simulated data shows differences between clustered (nonrandom) and random distribution of spots. The observed changes in the distribution of the Euclidean distances reports only on changes in the distribution of brightness because positional (x,y) information was kept constant. Relative to control samples, treatment of cells with either cytochalasin D or jasplakinolide shifted the curves of accumulated frequencies, as was observed with the simulated patterns.

Independently of the 2-D organization of the AChR in the plane of the membrane in the control samples (see below), treatments affected the arrangement of AChR nanoclusters as a function of their brightness. This finding suggests that disruption of the actin cytoskeletal

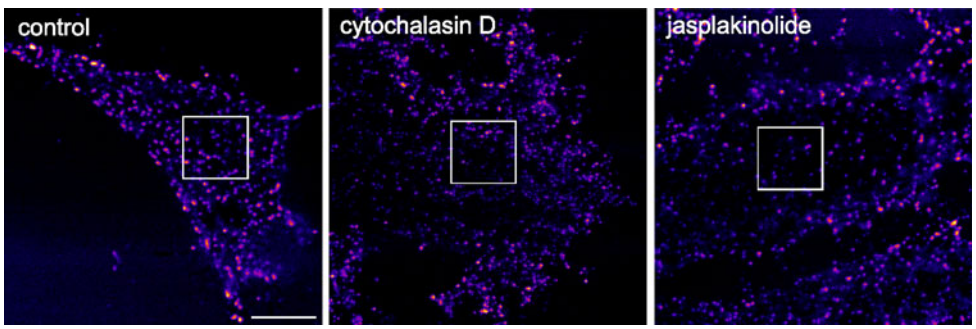

Fig. 2 Organization of the AChR at the cell surface of CHO-K1/A5 cells. STED images of CHO-K1/A5 cells incubated for 30 min at 37°C with complete medium only (control), cytochalasin D (2.5 µmol/l) or jasplakinolide (1 µmol/l). At the end of the incubation period cells were stained with mAb-210, an antibody against the AChR α subunit followed by Atto^{647N} secondary antibody, and fixation with 2% paraformaldehyde. Image analysis of the particles was performed on 5 × 5-µm regions of the cells (*central square*). *Lower right panels:* higher magnification of region of the cell membranes outlined by the rectangles. Scale bar = 2 µm

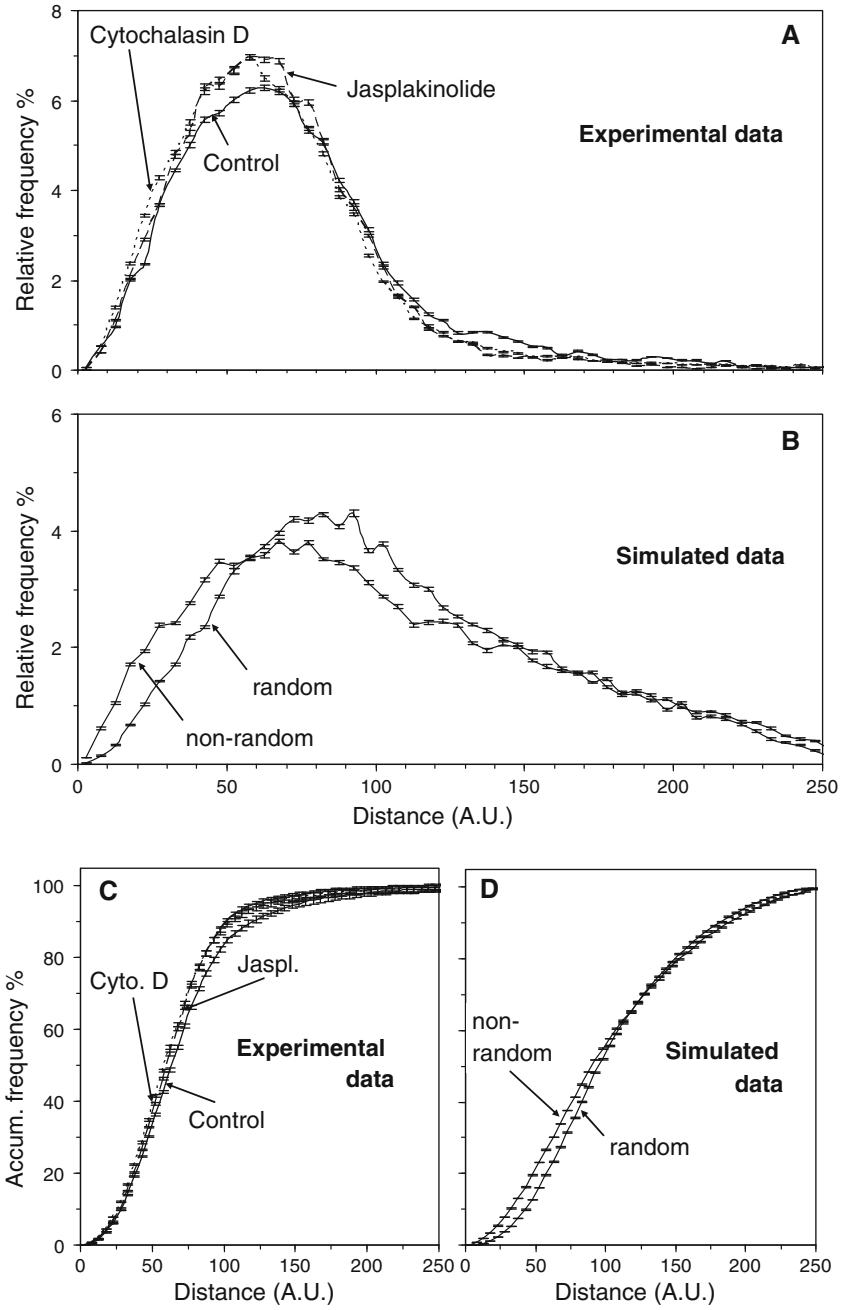

Fig. 3 Frequencies distribution of experimental (**a**, **c**) and simulated (**b**, **d**) data. Bars show SD

meshwork affects the spatial organization of the AChR nanoclusters according to their brightness/size, supporting the notion that receptor anchoring and distribution at the cell surface is coupled to the integrity of the cortical cytoskeleton.

Cytoskeletal-Disrupting Drugs Affect the Size and the Intrananocluster Density of AChRs

No differences were found in the brightness between control and treated samples either by direct examination of the median of brightness (35.4, 35.6, and 36.0) or applying Wilcoxon's test for comparison of the frequencies distribution (Fig. 4, left column). The lack of affectation of the brightness distribution after treatment of cells with cytoskeletal-disrupting drugs does not contradict the previous finding indicating that nanoclusters segregate according to their brightness/size. The latter involves spatial distribution of AChR nanoclusters according to their brightness, whereas the former involves the frequency distribution of brightness only, irrespective of their position in the plane of the membrane.

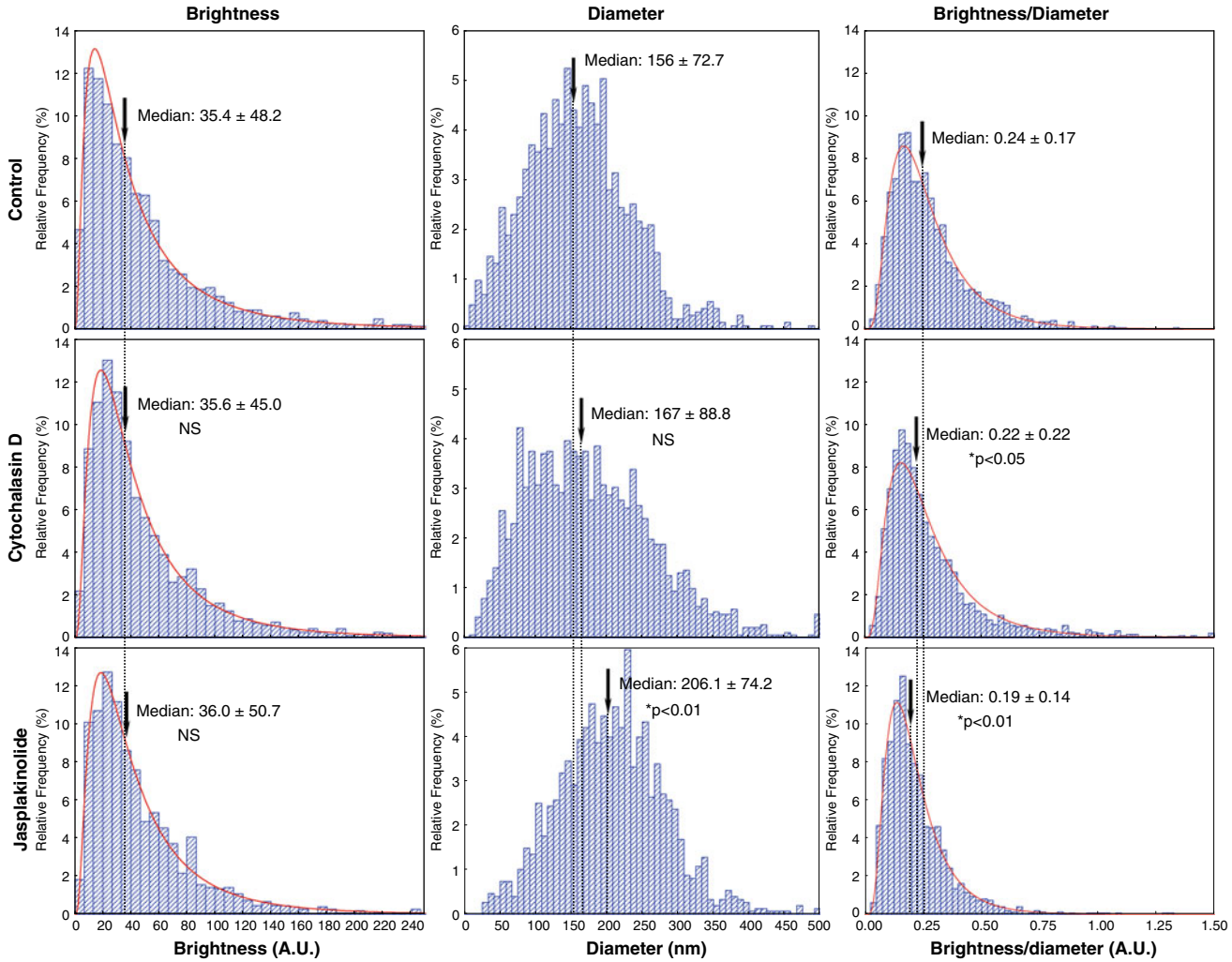

Fig. 4 Frequency distribution of brightness, diameter and brightness/diameter ratio in control and treated cells. When feasible, a log-normal distribution was fitted to the experimental data (*lines*). Arrows indicate the median and SD. Results of the Wilcoxon's test: *NS* statistically not significant; * significant at the correspondent level of significance (*P*)

Relative to control samples, the diameter of the nanoclusters was not significantly affected by treatment with cytochalasin D (Wilcoxon's test, NS). On the contrary, jasplakinolide treatment produced a significant increase ($P < 0.01$) in the diameter of clusters (Fig. 4, middle column). Careful examination of the histograms shows that the shift of the predominant frequencies to larger diameters (from 156 ± 72.7 to 206 ± 74.2 nm) in jasplakinolide-treated samples is mainly due to the diminution of the smaller diameters, i.e., below ~200 nm (left region of the histogram). This suggests that the drug acts mostly by dispersing small clusters and thereby increasing their diameter up to a medium value.

Assuming that the brightness of a fluorescent spot in the STED images is proportional to the amount of anti-mouse Atto^{647N}-labeled antibody bound to the AChR, the brightness/diameter ratio can be used as an approximate measure of the intrananocluster density of AChR molecules. The brightness/diameter ratio diminished after treatment with both cytochalasin D and jasplakinolide (Wilcoxon's test, $P < 0.05$ and $P < 0.01$, respectively, Fig. 4, right column), indicating a dispersion of particles within clusters. Because the brightness did not vary in a statistically significant manner after treatments (Fig. 4, left column), it follows that the reduction in the brightness/diameter ratio stems from the increase of the diameter of clusters (Fig. 4, middle column), but not to changes in brightness. Together, these findings reveal that both treatments—but more markedly in the case of jasplakinolide—cause an increase in the proportion of medium-size clusters at the expense of a reduction in the intrananocluster density of AChR molecules.

Spatial Organization of AChR Clusters According to Their Position in the Membrane

Ripley's Test

As shown in Fig. 5, the Ripley's $L(r) - r$ curve for the control samples fell within the interval for a random distribution. The minimum observed near the lower limit of the interval (i.e., -1) suggests, however, fewer distances around 200 nm (Fig. 5a). The curves for cytochalasin D and jasplakinolide fell outside the lower limit of confidence for a random distribution with minima at $\sim$200 and $\sim$300 nm, respectively, indicating fewer occurrences of these distances than those expected for a random distribution.

Ripley's analysis (Ripley 1977, 1979) is usually used to detect clustering of particles, in which case $L(r) - r$ is expected to be *higher* than the upper limit of the 99% CI at the typical distances of clustering, which indicates frequencies higher than those expected for a random pattern. Occasionally, particle clustering may yield curves above the upper 99% CI for most of the assayed distances (see, e.g., Fig. 7c). Patterns for which the $L(r) - r$ curve falls below the lower limit of the 99% CI implies shorter distances than expected for a random pattern. In a *simulated* arrangement, the distance between two simulated points (d) can range from zero to the value of the diagonal of the square box of size ℓ (i.e., $0 < d < \sqrt{2}\,\ell$) because points are dimensionless. However, in *real* images, any pair of particles cannot be separated by a distance shorter than the sum of their radii (see Supplementary Fig. 4). It can be inferred that this sum of radii corresponds to the prevailing diameter of the particles analyzed, and thus the portion of the $L(r) - r$ curve that falls below the 99% CI will be close to the prevailing particle diameter. Distances shorter than the mean diameter of the particles are less frequent than those expected for a simulated random distribution, and the minimum of the $L(r) - r$ curve will be located at distances (r) close to such size. Although the $L(r) - r$ function for treated samples fell below the lower 99% CI, experimental constraints made it impossible to establish whether the spatial distribution of AChR clusters (i.e., the central point of the ROIs) is random or not at distances below 500 nm for the control or treated samples. At larger distances

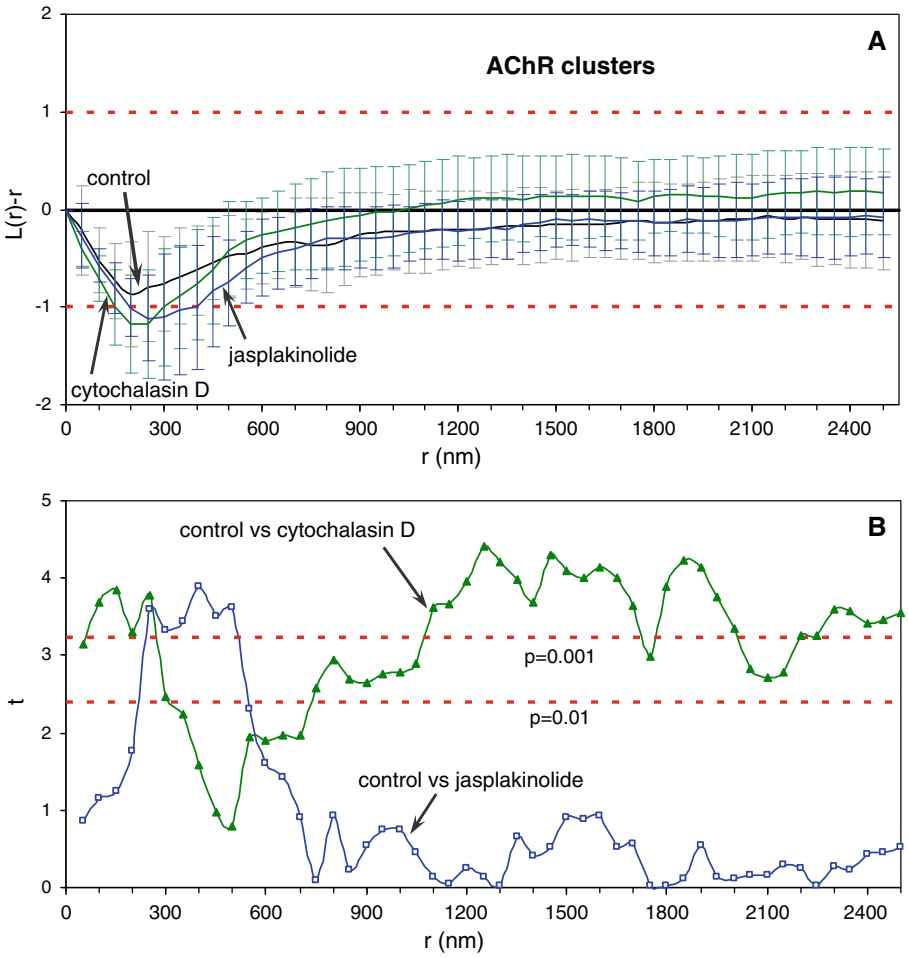

Fig. 5 **a** Ripley's analysis of the distribution of AChR clusters. Bars represent SD of the mean calculated from more than 60 STED images (see Supplementary Table 1). **b** The *t*-test comparing means of the Ripley's function $L(r) - r$ between control and treated samples. The t statistics was calculated for each distance; values above any of the *horizontal dotted lines* imply differences at the corresponding level of significance ($P < 0.001$ or $P < 0.01$)

(above ~500 nm), however, the distribution of AChR spots was random in all samples analyzed (Fig. 5a), as reported previously for control CHO-K1/A5 cells (Kellner et al. 2007). Thus, the randomness in the distribution of AChR nanoclusters in the membrane, at distances beyond ~500 nm, was not affected by disrupting the cytoskeleton with cytochalasin D or jasplakinolide (Fig. 5a).

The large number of replicates (more than 1400 clusters analyzed for each treatment; see Supplementary Table 1) compensates for the relatively large standard deviations in the Ripley's curves, enabling the application of the Student *t*-test. After corroboration of the normal distribution of the $L(r) - r$ values for each set of samples (control, cytochalasin D, and jasplakinolide), a requisite of applicability of the *t*-test, each experimental curve was compared with the control curve for all distances analyzed (Fig. 5b). Statistically significant differences ($P < 0.001$) were found between control and cytochalasin D-treated samples for distances below ~300 nm, and between control and jasplakinolide-treated samples for distances between ~250 and 500 nm. This comparison between Ripley's functions suggests that cytochalasin D and jasplakinolide affect the organization of AChR clusters, increasing the size of the AChR particles. Furthermore, although all samples exhibited a random distribution of clusters for distances above ~500 nm, the Ripley's function for cytochalasin D at distances above ~900 nm was significantly different in statistical terms from that of the control (Fig. 5b), indicating the occurrence of changes in the internanocluster distances.

Poisson Analysis

The organization of AChR clusters according to their position in the plane of the membrane was also investigated by means of Poisson analysis. For this purpose, the 5 × 5-μm selected regions in STED images were divided into square boxes of different sizes, and the clusters inside them were counted. The frequencies of boxes with a given number of clusters were then compared with the expected (random) frequencies. The χ^2 statistics were higher than the Chi_{crit} ($P < 0.01$) for control and treated samples in boxes of 500 × 500 nm (Fig. 6, left column), indicating statistically significant differences between the overall frequency distributions and the random distributions. The frequency of boxes with 1 and 0, 2, or 3 clusters was higher and lower, respectively, than expected for a random distribution. Upon increasing the box size to 1000 × 1000 nm (Fig. 6, right column), the χ^2 statistics were higher than the Chi_{crit} ($P < 0.01$) for control and jasplakinolide-treated cells, with a higher frequency of boxes with 1 particle. No statistically significant differences relative to a random distribution were found for cytochalasin D-treated samples at this box size, nor for either drug at the largest boxes evaluated (2500 × 2500 nm and 5000 × 5000 nm; data not shown).

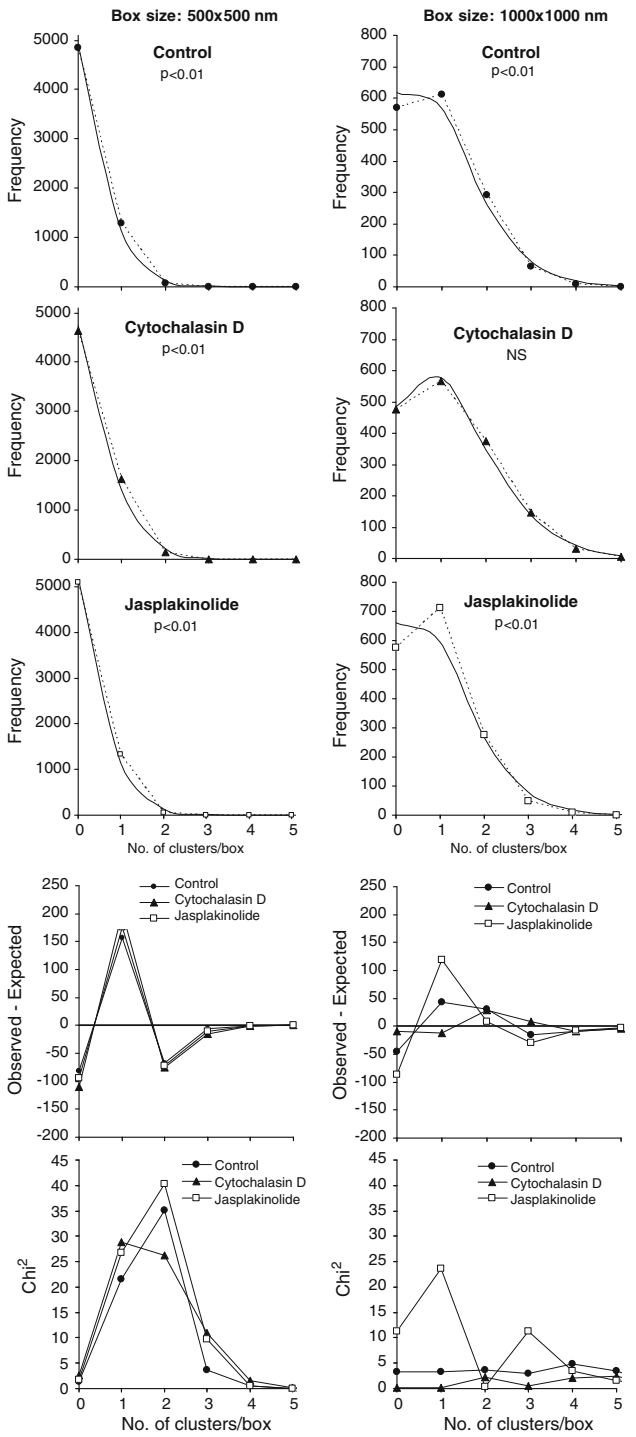

Fig. 6 Poisson analysis. *First and second columns* indicate frequencies of 500 × 500 nm and 1000 × 1000 nm boxes, respectively, as a function of the number of clusters per box. *Dotted lines,* observed frequencies; *solid lines,* expected frequencies for a random distribution (Poisson). *Third and fourth rows* indicate residuals and χ^2 statistics for each bin (a bin is a box with a given number of clusters—0, 1, 2, etc.)

The nonrandom distribution of AChR nanoclusters disclosed by the Poisson analysis brings into consideration the influence of nanocluster size. The fact that in 500 × 500-nm squares the Poisson analysis reveals more boxes with one nanocluster and fewer with two clusters than expected for a random distribution is consistent with nanocluster size in Ripley's analysis. The predominant diameter of clusters (Fig. 4, middle column) falls within this distance, and thus fewer clusters would fit within the 500 × 500–nm boxes. The frequency of boxes with two or more nanoclusters is thus lower than expected for a random distribution. The Poisson analysis (as also Ripley's) is conceived for the study of dimensionless particles, and its output must be carefully interpreted when applied to actual objects having a finite physical size. The nonrandomness of the AChR nanocluster distribution revealed here by the analysis provides information on the prevailing diameter of the nanoclusters.

Simulation of Intrananocluster Aggregation of AChR

The brightness of the AChR nanoclusters should depend on both the size and the number of AChR molecules within the nanocluster. To investigate the intrananocluster density of receptors in the experimental STED images, the expected number of receptors within each nanocluster was simulated. A "nanocluster brightness unit" was defined as the average brightness of the five nanoclusters with the lowest intensity in each image. The brightness of the remaining nanoclusters was next normalized relative to the brightness unit in each image and represented by a number (1, 2, 3, etc.) denoting the expected number of receptors (Fig. 7a). Because the resolution in STED images (∼75 nm) was not sufficient to dissect individual AChR macromolecules and their distribution within nanoclusters, the simulated molecules were distributed randomly inside the corresponding ROI of a nanocluster by custom-written software (crosses in Fig. 7b).

When Ripley's analysis was performed on the simulated patterns, the nonrandom distribution of the generated AChR molecules was apparent for all samples for distances as large as 2000 nm (Fig. 7c). This is not unexpected because the central point of each ROI (spot) is now surrounded by a number of simulated points representing the AChR molecules. The number of simulated AChR molecules within each nanocluster depends on the overall brightness of the nanocluster. Any pair of the simulated molecules could be separated by any distance (i.e., $0 < d < \sqrt{2}\,\ell$), and no $L(r) - r$ values below -1 should be expected. The highest degree of clustering occurs within the range 100–300 nm, matching the predominant diameter of the nanoclusters (see Fig. 4, middle column). This interval matches that in Ripley's analysis of STED images exhibiting a minimum (Fig. 5a) because the generated molecules are distributed within an ROI that initially had one "molecule" only.

When the $L(r) - r$ function of control and treated samples was compared in terms of the *t*-test for each distance, no statistically significant differences were found for samples treated with cytochalasin D (Fig. 7d). The $L(r) - r$ curve for jasplakinolide fell below the control values for a wide range of distances (<∼1500 nm), and the *t*-test revealed significant differences ($P < 0.01$) for distances shorter than ∼300 nm. This is consistent with the current hypothesis that the degree of aggregation of the intrananocluster AChR molecules diminishes after treatment with jasplakinolide, mainly in smaller clusters. The brightness, the intrananocluster density of particles and the area of a nanocluster (ROI) are closely related and mutually dependent, in agreement with the previous finding that drugs affect small clusters more strongly than larger ones. The range of distances concurs with the increase in the prevailing diameters of clusters and the decrease in the brightness/diameter ratio found after treatment with jasplakinolide (see Fig. 4, middle and right columns). Because treatments did not significantly affect the brightness (Fig. 4, left column), one may conclude that the reduction in the degree of aggregation of the AChR molecules within clusters caused by the drug is mainly due to the increase in the diameter of clusters and the subsequent dispersion of molecules.

Discussion

A mathematical analysis was performed on STED images of CHO-K1/A5 cells treated with drugs that disrupt the integrity of the cytoskeleton to investigate the role of the cortical cytoskeleton network on the spatial organization of AChR macromolecular aggregates and individual AChR molecules. The size-dependent output of the Ripley and Poisson analyses used to disclose the spatial organization of AChR clusters did not reveal whether their organization was random or not at relatively short distances (i.e., below 500 nm). To be able to establish this latter using the cited methods of spatial pattern analysis requires that the nanoclusters be small so as to avoid misinterpretation when contrasting the experimental data with the dimensionless clusters of the simulated patterns. Neither the Ripley nor the Poisson method is of use in cases where the particle size is large enough to match the distance at which the clusters occur. However, in agreement with previous results (Kellner et al. 2007), Ripley's analysis made it clear that the AChR clusters are randomly distributed at distances larger than ∼500 nm in all samples (Fig. 5a). The randomness of AChR nanocluster distribution in the

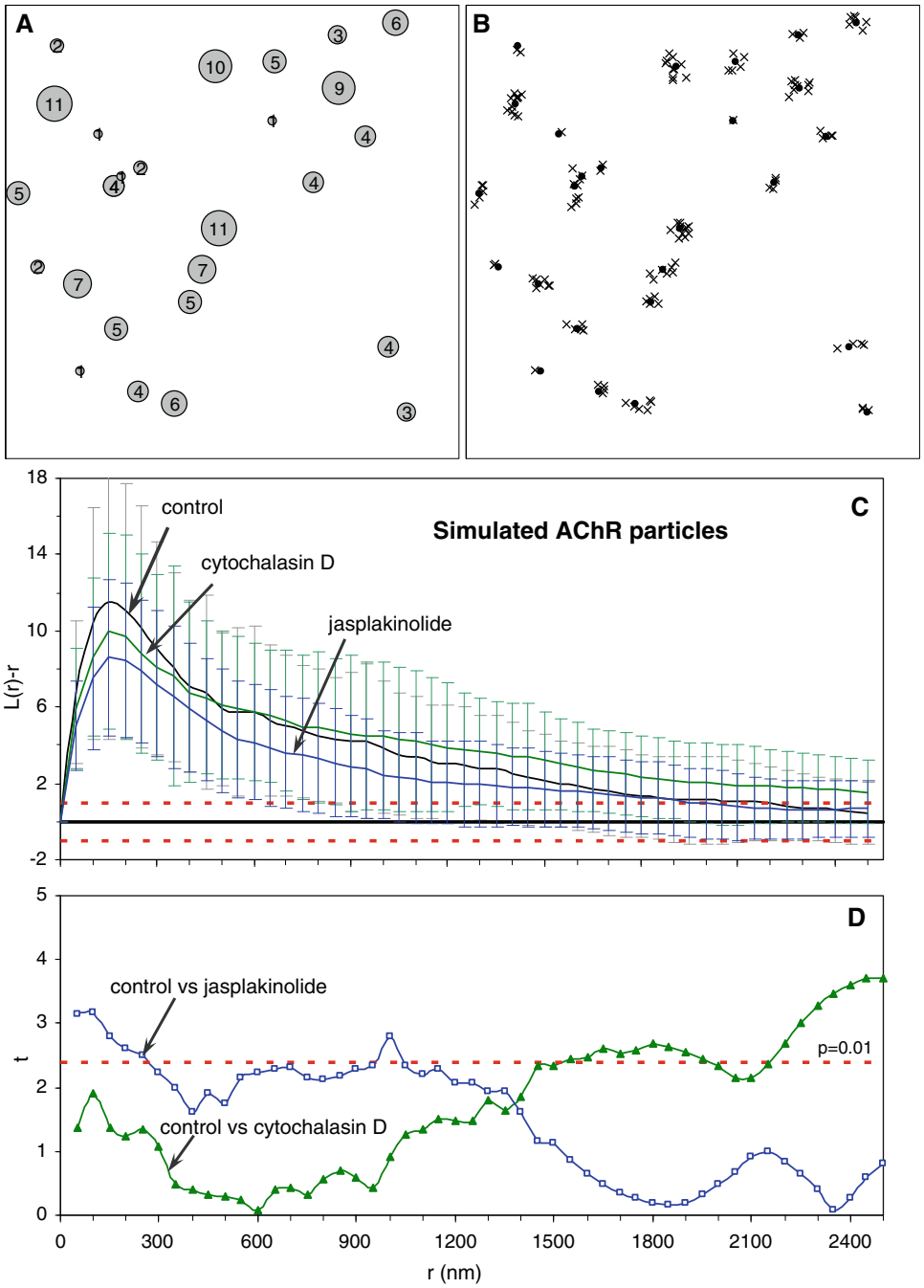

Fig. 7 Simulation of intrananocluster aggregation of AChR molecules. **a** Schematic depiction of particle distribution in a STED image, where the experimental brightness of the nanoclusters is proportional to the area of the circles. The figures represent the number of AChR particles generated for each cluster, calculated from the ratio between clusters brightness and the average brightness from the five clusters with the lowest brightness. **b** Generated particles (*crosses*) randomly distributed within the corresponding ROI. *Filled circles* correspond to the centroid of the ROIs. **c** Ripley's analysis on the generated particles. Bars = SD of the mean calculated from more than 60 STED images (see Supplementary Table 1). **d** The *t*-test for the mean comparison of $L(r) - r$ between control and treated samples. The *t*-statistics were calculated for each pair of distances; values above the dotted line imply differences at the corresponding level of significance ($P < 0.01$)

membrane between ~500 and 2500 nm was not altered upon disrupting the cytoskeleton with cytochalasin D or jasplakinolide (Fig. 5a). In contrast, cholesterol depletion of CHO-K1/A5 cells by cyclodextrin treatment led to a nonrandom distribution of AChR nanoclusters (Kellner et al. 2007). Whether the distribution of spacings larger than ~2500 nm is random or clustered is more difficult to establish because for a faithful Ripley output the analysis must be performed for distances smaller than half (i.e., 2500 × 2500 nm) of the selected portions (5 × 5 μm) in the microscope images. Given the nominal size (especially the width) of the CHO-K1/A5 cells, enlarging the regions under study is not advisable because this would include substrate cover glass and cell-free zones, potentially yielding fictitious clustering.

By means of different mathematical approaches, both cytochalasin D and jasplakinolide were found to alter the spatial organization of nanoclusters and AChR molecules, indicating that the cytoskeleton meshwork is involved in the anchoring and organization of the receptor in the membrane. Treatment with both drugs caused an increase in the prevailing size of clusters, whereas it did not

significantly affect the main brightness. Because the brightness can be assumed to be proportional to the number of AChR molecules within a nanocluster computed as the sum of the pixel intensities within the ROI, these findings can be explained in terms of a distribution of roughly the same number of AChR molecules within nanoclusters. Drugs may act by attacking the cytoskeleton network at multiple points in the anchoring system in the membrane, scattering the AChR aggregates and generating larger nanoclusters but with a similar number of particles. The increase in frequencies of medium-size nanoclusters and the reduction of small ones (less than $\sim$150 nm; see Fig. 4), especially in the case of jasplakinolide, can be accounted for by the stronger dispersing effects of the drugs on smaller clusters at the assayed concentration and exposure time.

On the basis of the present results, a possible size-dependent mechanism for the cytoskeleton-disrupting capability of the drugs can be hypothesized. The upper row in Fig. 8 shows a series of nanoclusters having the same number of AChR particles per unit area (i.e., density) but varying size, before being treated with the cytoskeleton-disrupting drugs. After treatment, AChR molecules are dispersed; the increase in area of the nanocluster is depicted as a gray ring. The smaller the original nanocluster size, the larger the relative area of the dispersion ring. Thus, smaller nanoclusters are more affected than larger ones. The reduction in the frequencies of the smaller nanoclusters in jasplakinolide-treated cells (Fig. 4, middle column) can thus be explained in terms of the dispersion of AChR molecules within the nanocluster, yielding medium-size clusters with lower density. The hypothetical mechanism of nanocluster disruption also explains why the frequencies of large nanoclusters did not vary significantly (Fig. 4, middle column). This size-dependent effect of the cytoskeleton-disrupting drugs could reflect the effective concentration of drugs at the site of action. For a given analytical concentration during treatments, the effective concentration of the drug at the site of action in the cells will depend on the ratio between the drug and the cytoskeletal proteins: the larger the size of the nanocluster, the lower the effective concentration of the drugs.

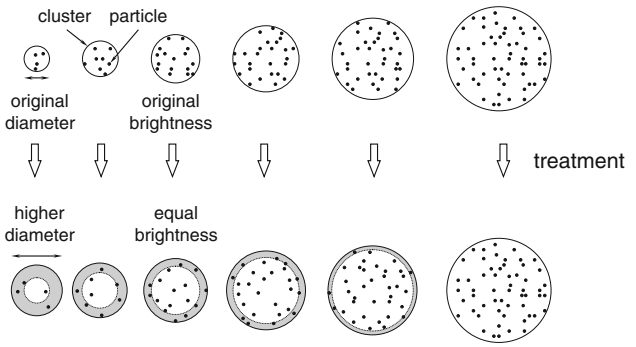

Fig. 8 Diagram illustrating the hypothetical mode of action of the two cytoskeletal-disrupting drugs cytochalasin D and jasplakinolide on nanocluster organization and their dependence on AChR nanocluster size. Six sizes of nanoclusters are schematically depicted in the top row, all having the same density of randomly distributed particles. The drugs disperse intrananocluster particles more effectively on smaller nanoclusters ($<\sim$150 nm), generating larger, medium-size nanoclusters with a similar number of particles. These changes are reflected in lower intrananocluster density, unchanged brightness, and lower brightness/diameter ratio. The model provides a reasonable explanation for the observed lack of variation in brightness, the increase in frequencies of middle-size clusters, and the decrease in the brightness/diameter ratios after treatments with the cytoskeletal-disrupting drugs, jasplakinolide in particular

Acknowledgments Thanks are due to Prof. S. H. Hell and his group for the use of the Leica TCS STED microscope at the facility of the Department of Nanobiophotonics, Max-Planck Institute for Biophysical Chemistry, Göttingen. Research described in this article was supported in part by PICT 01-12790 and 5-20155 from the Ministry of Science and Technology of Argentina; PIP no. 6367 from the Argentinian Scientific Research Council (CONICET); Philip Morris USA Inc., and Philip Morris International to F.J.B.

References

Appleyard ST, Witkowsky JA, Dipley BD, Shotton DM, Dubowitz V (1985) A novel procedure for pattern analysis of features present on freeze-fractured plasma membranes. J Cell Sci 74:105–117

Barrantes FJ (1983) Recent developments in the structure and function of the acetylcholine receptor. Int Rev Neurobiol 24:258–341

Barrantes FJ (2007) Cholesterol effects on nicotinic acetylcholine receptor. J Neurochem 103(suppl 1):72–80

Borges LS, Yechikhov S, Lee YI, Rudell JB, Friese MB, Burden SJ, Ferns J (2008) Identification of a motif in the acetylcholine receptor beta subunit whose phosphorylation regulates rapsyn association and postsynaptic receptor localization. J Neurosci 28:11468–11476

Borroni V, Baier CJ, Lang T, Bonini I, White MM, Garbus I, Barrantes FJ (2007) Cholesterol depletion activates rapid internalization of submicron-sized acetylcholine receptor domains at the cell membrane. Mol Membr Biol 24:1–15

Brockhausen J, Cole RN, Gervásio OL, Ngo ST, Noakes PG, Phillips WD (2008) Neural agrin increases postsynaptic ACh receptor packing by elevating rapsyn protein at the mouse neuromuscular synapse. Dev Neurobiol 68:1153–1169

Brusés JL, Chauvet N, Rutishauser U (2001) Membrane lipid rafts are necessary for the maintenance of the alfa-7 nicotinic acetylcholine receptor in somatic spines of ciliary neurons. J Neurosci 21:504–512

Bubb MR, Senderowicz AM, Sausville EA, Duncan KL, Korn ED (1994) Jasplakinolide, a cytotoxic natural product, induces actin polymerization and competitively inhibits the binding of phalloidin to F-actin. J Biol Chem 269:14869–14871

Choquet D, Triller A (2003) The role of receptor diffusion in the organization of the postsynaptic membrane. Nat Rev Neurosci 4:251–265

Cooper JA (1987) Effects of cytochalasin and phalloidin on actin. J Cell Biol 105:1473–1478

Fuhrer C, Gautam M, Sugiyama JE, Hall ZW (1999) Roles of rapsyn and agrin in the interaction of postsynaptic proteins with acetylcholine receptors. J Neurosci 19:6405–6416

Hell SW, Wichmann J (1994) Breaking the diffraction resolution limit by stimulated emission. Opt Lett 19:780–782

Kellner R, Baier J, Willig KI, Hell SW, Barrantes FJ (2007) Nanoscale organization of nicotinic acetylcholine receptors revealed by STED microscopy. Neuroscience 144:135–143

Klar TA, Hell SW (1999) Subdiffraction resolution in far-field fluorescence microscopy. Opt Lett 24:954–956

Kumari S, Borroni V, Chaudhry A, Chanda B, Massol R, Mayor S, Barrantes FJ (2008) Nicotinic acetylcholine receptor is internalized via a Rac-dependent, dynamin-independent endocytic pathway. J Cell Biol 181:1179–1193

Kummer TT, Misgeld T, Sanes JR (2006) Assembly of the postsynaptic membrane at the neuromuscular junction: paradigm lost. Curr Opin Neurobiol 16:74–82

Marangi PA, Forsayeth JR, Mittaud P, Erb-Vögtli S, Blake DJ, Moransard M, Sander A, Fuhrer C (2001) Acetylcholine receptors are required for agrin-induced clustering of postsynaptic proteins. EMBO J 20:7060–7073

Marchand S, Devillers-Thiery A, Pons S, Changeux JP, Cartaud J (2002) Rapsyn escorts the nicotinic acetylcholine receptor along the exocytic pathway via association with lipid rafts. J Neurosci 22:8891–8901

Ripley BD (1977) Modelling spatial patterns. J R Stat Soc B 39:172–192

Ripley BD (1979) Test of randomness for spatial point patterns. J R Stat Soc B 41:368–374

Roccamo AM, Pediconi MF, Aztiria E, Zanello L, Wolstenholme A, Barrantes FJ (1999) Cells defective in sphingolipid biosynthesis express low amounts of muscle nicotinic acetylcholine receptor. Eur J Neurosci 11:1615–1623

Sadasivam G, Willmann R, Lin S, Erb-Vögtli S, Kong XC, Rüegg MA, Fuhrer C (2005) Src-family kinases stabilize the neuromuscular synapse in vivo via protein interactions, phosphorylation, and cytoskeletal linkage of acetylcholine receptors. J Neurosci 25:10479–10493

Sieber JJ, Willig KI, Kutzner C, Gerding-Reimers C, Harke B, Donnert G, Rammner B, Eggeling C, Hell SW, Grubmuller H, Lang T (2007) Anatomy and dynamics of a supramolecular membrane protein cluster. Science 317:1072–1076

Willman R, Pun S, Stallmach L, Sadavisam G, Ferrao Santos A, Caroni P, Fuhrer C (2006) Cholesterol and lipid microdomains stabilize the postsynapse at the neuromuscular junction. EMBO J 25:4050–4060